Exploring Isomerism in Isolated Cyclodextrin Oligomers through Trapped Ion Mobility Mass Spectrometry

Papri Chakraborty,* Marco Neumaier, Patrick Weis, and Manfred M. Kappes*

ABSTRACT: Cyclodextrin (CD) macrocycles are used to create a wide range of supramolecular architectures which are also of interest in applications such as selective gas adsorption, drug delivery, and catalysis. However, predicting their assemblies and identifying the possible isomers in CD oligomers have always remained challenging due to their dynamic nature. Herein, we interacted CDs (α, β, and γ) with a divalent metal ion, Cu^{2+}, to create a series of Cu^{2+}- linked CD oligomers, from dimers to pentamers. We characterized these oligomers using electrospray ionization mass spectrometry and probed isomerism in each of these isolated oligomers using high resolution trapped ion mobility spectrometry. Using this technique, we separated multiple isomers for each of the Cu^{2+}-interlinked CD oligomers and estimated their relative population, which was not accessible previously using other characterization techniques. We further carried out structural analysis of the observed isomers by comparing the experimental collision cross sections (CCSs) to that of modeled structures. We infer that the isomeric heterogeneity reflects size-specific packing patterns of individual CDs (e.g., close-packed/linear). In some cases, we also reveal the existence of kinetically trapped structures in the gas phase and study their transformation to thermodynamically controlled forms by examining the influence of activation of the ions on isomer interconversion.

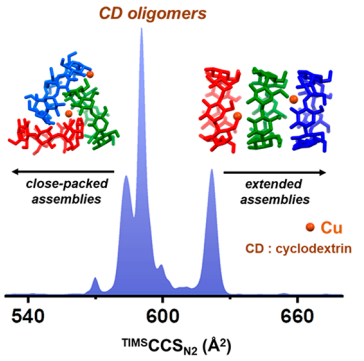

INTRODUCTION

Self-assembled nano- and microstructures comprising macrocycles are of growing interest in different areas of chemical sciences. Among these, cyclodextrins (CDs) attract particular attention because of their nontoxic nature, high stability, and numerous applications.[1−3] CDs (α, β, and γ depending on the ring size) are cyclic oligosaccharides, which are toroidal in shape with a wider secondary (head/H) and a narrower primary (tail/T) rim encircled by hydroxyl groups. CDs exhibit high affinity for the formation of inclusion complexes with various organic guests and are also used in designing mechanically interlocked molecules,[4] metal organic frameworks,[5] and supramolecular polymers,[6] which are central areas of interest in molecular self-assembly.

The assembly of CDs can be strongly influenced by interaction with a variety of metal ions ranging from monovalent to pentavalent.[7] The interaction of CDs with Cu(II) ions has been widely investigated in this regard.[8−10] For instance, multinuclear Cu-bound sandwich type dimeric complexes have been observed in condensed phase studies.[11,12] Stoddart and co-workers reported the crystal structure of $[Na_4Cu_4(\gamma\text{-}CDH_{-3})_4(OH_2)]$ which consists of two unsymmetrical sandwich type dimeric CD units.[11] Although some ordered arrangements are observed in crystals, predicting the assembly of such metal-ion-linked, CD-based molecular systems in solution or in gas-phase remains challenging. Computational studies have been used to predict the structural dynamics in CD dimers.[13,14] For higher oligomers containing more than two CDs, it is even more challenging to predict the isomers as different possible relative orientations of the truncated-cone shaped CDs lead to a huge potential isomer space. Despite the rapidly increasing efforts in designing precision oligomeric structures for applications, little size-specific experimental information on CD oligomers is so far available. The difficulty arises due to the intrinsically polydisperse nature of aggregates generated by condensed phase or solution phase synthesis. Moreover, X-ray crystallography resolves only the dominant state in such samples. Techniques like electron microscopy, nuclear magnetic resonance spectroscopy, or other spectroscopic methods mostly provide ensemble averaged structural information. By contrast, ion mobility mass spectrometry (IM MS) can provide information on the isomeric states of isolated monomers and of mass-selected and therefore size-selected oligomers.[15−20]

IM MS can distinguish different isomers of a mass-selected molecular ion because differences in isomer shape are reflected by differences in the measured collision cross sections (CCS). These isomer-resolved CCS distributions can then be

compared with calculated structures to determine their structures. IM MS is known to be a powerful tool to study complex topologies of charged supramolecular assemblies.[21,22] Very recently IM MS has also been used to begin to explore structures of CDs interacting with alkali metal cations[23,24] and to characterize various host–guest complexes of CDs in the gas phase.[25,26]

Herein, we utilized the interaction of CDs ($\alpha/\beta/\gamma$) with a divalent metal ion, Cu^{2+}, to create a series of cationic CD oligomers (up to pentamers) with varying (CD:Cu) stoichiometries. We characterized these oligomers using electrospray ionization (ESI) MS and explored their isomerism using trapped ion mobility spectrometry (TIMS), an instrumental IM variant which separates isomeric ions with high CCS resolution (~200) and provides highly accurate CCS values.[27,28] Our investigations demonstrate that TIMS MS can be used as an efficient analytical technique to identify size-specific isomerism in isolated Cu^{2+}-interlinked CD oligomers. We further reveal that this isomer space is dependent on the nature of the CD ($\alpha/\beta/\gamma$). To assign structures of the isomers, we compared the experimental CCS data to that of structural models based on different levels of theory ranging from semiempirical to density functional theory (DFT). For this, theoretical CCS values of the modeled structures were determined using trajectory method (TM) calculations. The so-derived size-specific evolution of CCS of the oligomers provided insight into the overall growth pattern. We also explored how these isomer populations can be influenced by experimental parameters.

MATERIALS AND METHODS

Sample Preparation. The reagents α, β, and γ cyclodextrins (>97% purity) and copper(II) nitrate were purchased from Sigma-Aldrich. CDs ($\alpha/\beta/\gamma$) and $Cu(NO_3)_2$ were mixed in equimolar quantities to prepare 1 mM solutions in a solvent mixture of water and acetonitrile (1:1 v/v).

Trapped Ion Mobility Spectrometry (TIMS). TIMS MS studies were performed using a commercial Bruker timsTOF instrument, coupled with an electrospray source. All measurements were carried out in the positive ion mode in the mass range 500–3000 m/z, with a mass resolution of >25 000. Electrospray conditions of capillary voltage 3000–4000 V, end plate offset 2000 V, nebulizer 0.3 bar, drying gas 3.5 L/min, dry temperature 200 °C, and flow rate 3 μL/min were used. The other general settings used were the following: funnel 1 RF, 300 Vpp; funnel 2 RF, 300 Vpp; multipole RF, 300 Vpp; isCID energy, 0 V; deflection delta, 70 V; quadrupole ion energy, 6 eV; collision cell energy, 6 eV; collision RF, 1000 Vpp; transfer time, 100 μs; prepulse storage, 20 μs.

High mobility resolution (~150–200) (in N_2) was achieved by measuring with an inverse mobility gap $\{(1/K_0\ \text{End}) - (1/K_0\ \text{Start})\}$ of 0.3 Vs/cm^2 and ramp time of 500 ms. The accumulation time was 20 ms. TIMS voltages were as follows: $\Delta1$ = 0 V, $\Delta2$ = 80 V, $\Delta3$ = 20 V, $\Delta4$ = 20 V, $\Delta5$ = 0 V, and $\Delta6$ = 20 V. The "tunnel in" pressure was 2.5 mbar, and the "tunnel out" pressure was 0.78 mbar. After the mobility separation, the ions of interest were mass selected via a RF quadrupole before the time-of-flight analysis and finally reaching the detector. TIMS does not provide absolute CCS values like drift tube IM. In TIMS, a calibration is needed to obtain the CCS of the ions. For this, commercially available "tune mix" from Agilent and drift tube CCS values of the calibrant reported by Stow et al. were used.[29] TIMS provides measurements of relative ion intensities versus inverse mobilities ($1/K$), which were then converted to CCSs following the Mason–Schamp equation (to yield mobilograms). The corresponding $^{TIMS}CCS_{N2}$ values reported here were averaged over three independent measurements. To study the dependence of the relative intensities of the isomers on the instrumental voltages, the ions were activated by varying the source conditions (capillary voltage and end plate offset) or the TIMS voltages, as specified in appropriate cases.

Calculations To Generate Model Structures and Theoretical CCS. The semiempirical PM7 method,[30] implemented in MOPAC,[31] which also considers hydrogen bonding (HB) interactions, was used for optimization of the model structures. The CCSs of the calculated structures were determined using the TM in IMOS ($^{TM}CCS_{N2}$).[32] As the drift gas N_2 is anisotropic, the ion–quadrupole interactions (qpol)[33] were also taken into account. For the monomers, we also validated the results on geometries obtained by DFT calculations. The theoretical CCSs obtained on DFT and PM7 optimized monomer geometries were in agreement with each other within 2%, which is also in the range of accepted deviation between experimental and calculated CCS. For the larger oligomers, geometry optimizations were performed only at the PM7 level for computational efficiency. Note that the objective here was to contrast theoretical CCS of different plausible model structure topologies with the experimental CCS and not detailed studies on isomer stabilization or binding energies. Further details on the calculations are provided in the Supporting Information.

RESULTS AND DISCUSSION

We present our results mainly focusing on β-CD. β-CD is known to show a higher tendency of aggregation than α and γ-CDs which we also compare with below.

ESI MS of Cu(II)-Linked Oligomers of β-CDs. A typical ESI mass spectrum of a 1:1 mixture of β-CD:Cu^{2+} is presented in Figure 1. Pronounced oligomerization up to pentamers was observed. In the following, these oligomers are represented as $(n{:}m)^{z+}$ where n and m are the number of CD and Cu units, respectively, and z is the overall charge state. A complete compositional assignment of the oligomeric peaks for β-CD is presented in Table 1. It has been shown in condensed phase

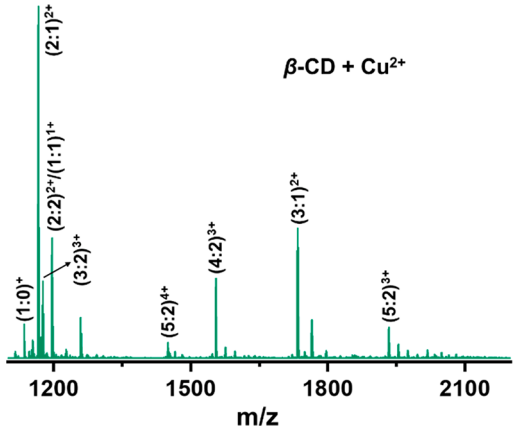

Figure 1. ESI MS of a 1:1 mixture of β-CD and Cu^{2+}. The peaks are denoted as $(n{:}m)^{z+}$ where n and m are the number of (correspondingly deprotonated) β-CD and Cu^{2+}, respectively, and z is the overall charge of the complex.

Table 1. List of Cu^{2+} Induced Oligomeric Peaks of β-CD Showing Their m/z Values, Molecular Formulas, $^{TIMS}CCS_{N2}$ (Å^2), and Relative Intensities of the Isomers of Each of the Oligomers

species	m/z	molecular formula	isomer	$^{TIMS}CCS_{N2}$ (Å^2)	relative intensity
$(1:0)^{1+}$	1136	$[(\beta\text{-CD})H]^+$	i	308	1.00
$(1:1)^{1+}$	1197	$[(\beta\text{-CD})CuH_{-1}]^{1+}$	i	309	1.00
$(1:1)^{2+}$	599	$[(\beta\text{-CD})Cu]^{2+}$	i	341	1.00
$(2:1)^{2+}$	1167	$[(\beta\text{-CD})_2Cu]^{2+}$	i	447	0.31
			ii	461	0.17
			iii	473	1.00
$(2:2)^{2+}$	1197	$[(\beta\text{-CD})_2Cu_2H_{-2}]^{2+}$	i	478	0.99
			ii	482	1.00
$(3:1)^{2+}$	1734	$[(\beta\text{-CD})_3Cu]^{2+}$	i	584	1.00
$(3:2)^{3+}$	1177	$[(\beta\text{-CD})_3Cu_2H_{-1}]^{3+}$	i	585	0.45
			ii	592	1.00
			iii	623	0.47
$(4:2)^{3+}$	1555	$[(\beta\text{-CD})_4Cu_2H_{-1}]^{3+}$	i	682	1.00
			ii	688	0.96
			iii	699	0.22
			iv	714	0.40
			v	720	0.35
$(5:2)^{3+}$	1934	$[(\beta\text{-CD})_5Cu_2H_{-1}]^{3+}$	i	770	0.74
			ii	792	1.00
			iii	813	0.27
$(5:2)^{4+}$	1450	$[(\beta\text{-CD})_5Cu_2]^{4+}$	i	793	0.10
			ii	805	0.38
			iii	821	0.54
			iv	838	1.00

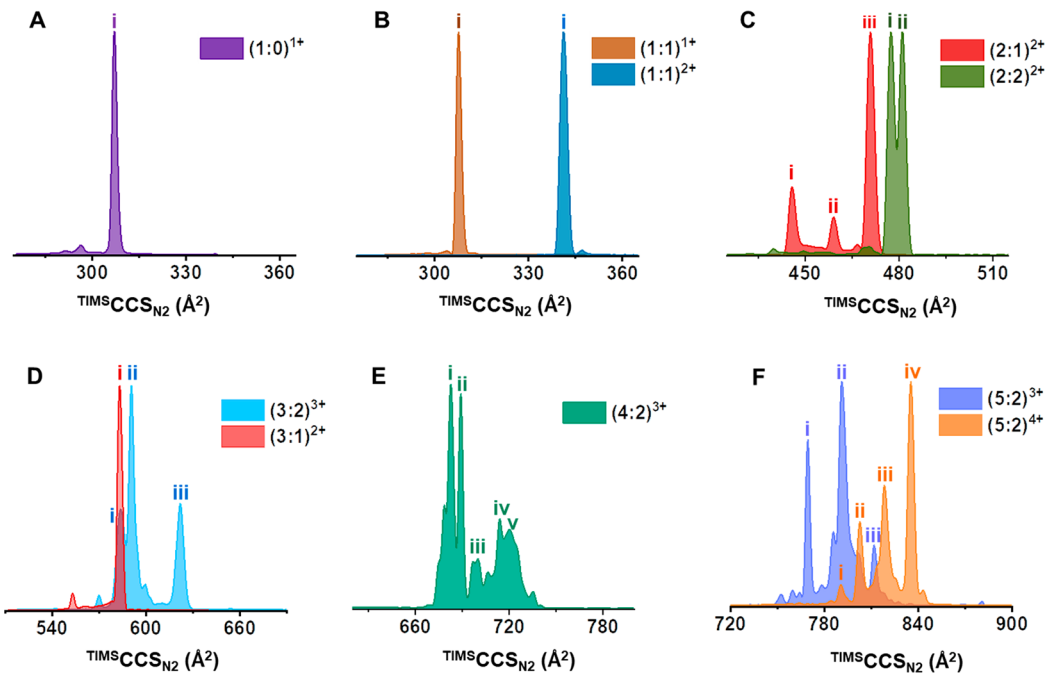

Figure 2. TIMS mobilograms of (A) protonated β-CD monomer, and Cu-linked β-CD (B) monomers, (C) dimers, (D) trimers, (E) tetramers, and (F) pentamers. Oligomers are denoted as $(n{:}m)^{z+}$ where n and m are the number of (correspondingly deprotonated) β-CD and Cu^{2+}, and z is the overall charge state of the species, respectively.

studies that interaction of Cu ions with CDs can occur through deprotonated −OH groups of CDs.[7,12] Here, our mass resolution allows us to clearly distinguish the number of such deprotonations, which is implicit in the $(n{:}m)^{z+}$ nomenclature (see Table 1). CDs being neutral molecules, the overall charge on $(n{:}m)^{z+}$ species arises from the charge on Cu (2+) and the number of deprotonations (−1). The doubly charged dimer of β-CD, $(2:1)^{2+}$ (m/z 1167), was the most abundant peak in the mass spectrum. Other dimers like the doubly deprotonated $(2:2)^{2+}$ (m/z 1197) were also observed. Multiple charged trimers $(3:2)^{3+}$ (m/z 1177), $(3:1)^{2+}$ (m/z 1734); tetramers $(4:2)^{3+}$ (m/z 1555); and pentamers $(5:2)^{4+}$ (m/z 1450), $(5:2)^{3+}$ (m/z 1934) were detected in reasonable intensities. The peak at m/z 1136 corresponded to monomeric

protonated β-CD, $(1{:}0)^{1+}$. The $(2{:}2)^{2+}$ dimer signal also contained some contribution of the monomer $(1{:}1)^{1+}$ at the same m/z value (which was separated using TIMS MS, as will be discussed in the following sections). A peak for $(1{:}1)^{2+}$ was also observed at m/z 599 in the low mass region (Figure S1A). ESI MS of protonated β-CD (i.e., without $Cu(NO_3)_2$ added to the solution), presented in Figure S1B, showed a dominant peak only for the monomer $(1{:}0)^{1+}$ (m/z 1136), which indicated that oligomeric complexes were not formed in the absence of the Cu^{2+} ions. Moreover, the relative intensities of the $(n{:}m)^{z+}$ complexes were also similar under different electrospray conditions (Figure S2). The experimental isotopic distributions of the $(n{:}m)^{z+}$ peaks were compared with their simulated patterns to further confirm the assignments (Figure S3).

TIMS MS of β-CD Based Monomers and Cu^{2+}-Linked Oligomers. TIMS mobiligram of the protonated β-CD monomer, $(1{:}0)^{1+}$, revealed one major peak with a CCS value of 308 Å^2 ($^{TIMS}CCS_{N2}$, Figure 2A), consistent with the previously reported drift tube CCS value of 312 Å^2.[34] Similarly, the $(1{:}1)^{+}$ complex showed a single peak with $^{TIMS}CCS_{N2}$ of 309 Å^2 (Figure 2B), suggesting that addition of one Cu ion does not have a significant effect on the CCS. The $(1{:}1)^{2+}$ species also showed one dominant form (Figure 2B) with $^{TIMS}CCS_{N2}$ of 341 Å^2. The larger CCS of $(1{:}1)^{2+}$ compared to $(1{:}1)^{1+}$ can be attributed to charge effects as the ion-induced dipole and ion-quadrupole interaction between the ion and N_2 depends on the partial charge distribution. Next, we turn to the oligomers, where individual CD units may differ in their relative orientation resulting in numerous possible conformational/topological isomers. TIMS MS clearly revealed the existence of multiple isomers in $(n{:}m)^{z+}$ (n = 2−5) oligomers as shown in Figure 2C−F. $^{TIMS}CCS_{N2}$ values of the different isomers (denoted as i, ii, iii, etc. in Figure 2) of the $(n{:}m)^{z+}$ species are summarized in Table 1. Three distinct isomers were observed for $(2{:}1)^{2+}$ dimer with $^{TIMS}CCS_{N2}$ of 447, 461, and 473 Å^2, whereas two isomers were observed for $(2{:}2)^{2+}$ with very close $^{TIMS}CCS_{N2}$ values of 478 and 482 Å^2 (Figure 2C). This indicated that the number of Cu ions (m) in a particular size (n) of an oligomer also controls the isomer distribution. For the trimer $(3{:}1)^{2+}$, one dominant isomer was observed with $^{TIMS}CCS_{N2}$ of 584 Å^2, whereas for $(3{:}2)^{3+}$, three major isomers were observed with $^{TIMS}CCS_{N2}$ of 585, 592, and 623 Å^2 (Figure 2D). The tetramer $(4{:}2)^{3+}$ showed two dominant isomers with $^{TIMS}CCS_{N2}$ of 682 and 688 Å^2 along with the contribution of some extended forms at $^{TIMS}CCS_{N2}$ ∼ 699−720 Å^2 (Figure 2E). Similarly, three (770, 792, and 813 Å^2) and four (793, 805, 821, and 838 Å^2) major isomers were observed for the pentamers $(5{:}2)^{3+}$ and $(5{:}2)^{4+}$, respectively (Figure 2F). TIMS MS experiments were repeated several times on freshly mixed solutions, and the absolute error in the values of $^{TIMS}CCS_{N2}$ was ∼1.0%, whereas the relative error in $^{TIMS}CCS_{N2}$ of the different isomers of a particular $(n{:}m)^{z+}$ species was ∼0.2%, respectively. The relative intensities of the isomers (see Table 1) which reflects their population in the gas-phase were also similar (within an error limit of 0.2%) when measured on different days under same concentration and spray conditions on freshly mixed solutions. Although we present the isomer abundance in terms of their relative intensities, the recorded overall intensities of the TIMS MS spectra were reasonably high (∼10^5−10^7 counts on peak maxima), giving high signal-to-noise ratios (Figure S4). Isomers with an intensity of ≲10% of the most abundant form of $(n{:}m)^{z+}$ species are not considered. Also, in the cases of tetramers and pentamers, which show a greater number of isomers, certain shoulder features, although at an intensity >10%, are not considered to reduce the complexity in analyzing the spectra. The relative intensities of the isomers of $(n{:}m)^{z+}$ did not show significant changes while changing the electrospray conditions like source voltages (Figures S5−S8), except some small effects for $(2{:}2)^{2+}$ (Figure S6, this will be addressed in more detail in the later sections) and $(4{:}2)^{3+}$ (Figure S8A). This indicated that the isomeric ions are robust and stable and separated from other topologies by high interconversion energy barriers, generally not surmountable under the experimental conditions.

Structures of β-CD Based Monomers. β-CD monomers may show different isomers depending on the relative orientation of the hydroxyl groups at their primary and secondary rims.[35] In the crystal structures of β-CD, the primary −OHs are mostly oriented outward and the primary rim remains open (open monomer, Figure S9A). However, earlier reports on calculated structures of neutral β-CD monomers in vacuum suggest the most stable isomer to have all seven primary −OHs rotated inward, closing the primary rim by an alcohol-heptamer type, extensive H-bonded pattern (closed monomer, see Figure S9B).[36,37] To study the probable structures of $(1{:}0)^{1+}$, we considered protonation on different possible sites, i.e., secondary −OH, primary −OH, glycosidic O, and glucose ring O, of the closed (M1−M4) and open type (M5−M8) β-CD structures. The PM7 optimized geometries of the isomeric structures of $(1{:}0)^{1+}$ are presented in Figures S10 and S11. $^{TM}CCS_{N2}$ values of closed isomers (M1−M4) were ∼314−319 Å^2 (Figure S10), and the open isomers (M5−M8) were ∼323−325 Å^2 (Figure S11). This indicated that although the open and closed forms of the monomers are distinguishable by TIMS MS, changes in the protonation site do not have a significant effect on CCS and hence are not distinguishable. $^{TM}CCS_{N2}$ of the lowest energy closed structure, M1 (Figure 3A), is 314 Å^2, which is in good agreement with the experimental CCS of 308 Å^2 (within 2%). In contrast, the lowest energy open type isomer, M5 (Figure 3B), showed $^{TM}CCS_{N2}$ of 325 Å^2 and exhibited larger deviation (∼5.5%) from the experiment. This suggests that the closed form of $(1{:}0)^{1+}$ is observed in TIMS MS experiments. The closed isomer (M1) is also energetically more favorable by 1.75 eV compared to M5 (Table S1). We further performed geometry optimization on M1 and M5 at the DFT level which also showed similar trends in CCS and energies like PM7 calculations (Figure S12).

Similarly, in the case of the Cu-bound β-CD monomers $(1{:}1)^{1+}$ and $(1{:}1)^{2+}$, we considered different isomeric structures with Cu^{2+} binding at primary and secondary −OH groups of both open and closed forms of β-CD monomer (Figures S13 and 14, Tables S2 and S3). Here also, the closed-type structures of the monomers showed best agreement to experimental CCS. The lowest energy closed-type structure of $(1{:}1)^{1+}$ showed $^{TM}CCS_{N2}$ of 315 Å^2 (Figure S13), consistent with $^{TIMS}CCS_{N2}$ value of 309 Å^2. The most stable closed structure of $(1{:}1)^{2+}$ showed $^{TM}CCS_{N2}$ of 340 Å^2 (Figure S14) in agreement with $^{TIMS}CCS_{N2}$ of 341 Å^2.

Isomers of Cu^{2+}-Linked β-CD Dimers. Different CD dimer topologies are possible depending on the orientation of the monomers. Bonnet et al. performed molecular modeling studies on neutral β-CD dimers in the gas phase and showed that HH orientation is preferred.[14] To model $(2{:}1)^{2+}$, we

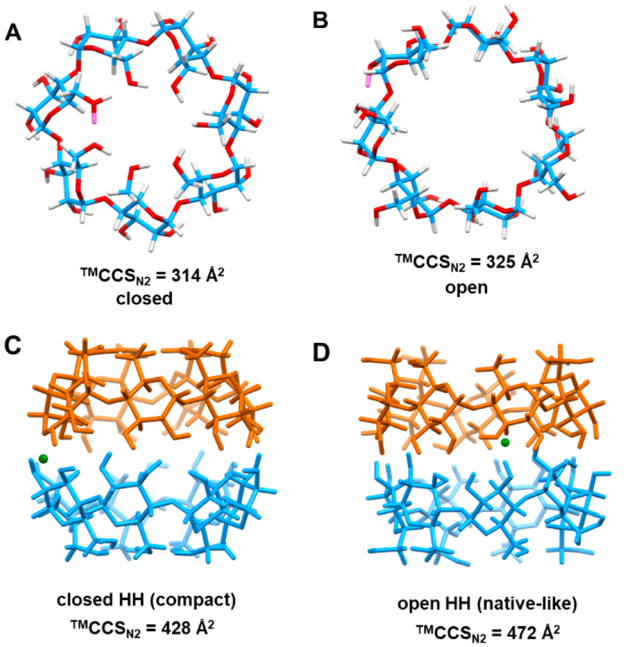

Figure 3. PM7 optimized geometries of (A) closed $(1{:}0)^{1+}$ β-CD monomer (M1), (B) open β-CD monomer (M5), (C) closed HH compact $(2{:}1)^{2+}$ β-CD dimer (D1), and (D) open HH native-like $(2{:}1)^{2+}$ β-CD dimer (D2). Color codes: (in parts A and B) blue, C; red, O; gray, H; purple, proton; (in parts C and D) β-CD rings are colored in blue/orange for the clarity of presentation; green, Cu.

therefore first considered a HH dimer using the primary closed-type monomer β-CD structure discussed above. This compact, Cu^{2+}-linked, closed-type HH dimer, D1, shown in Figure 3C, has $^{TM}CCS_{N2}$ of 428 Å^2, which is close to the smallest experimentally observed isomer i ($^{TIMS}CCS_{N2}$ = 447 Å^2) of $(2{:}1)^{2+}$ (Figure 2C). The other isomers (ii, iii) of $(2{:}1)^{2+}$ in TIMS MS showed larger CCS, suggesting that they may involve open-type HH structures of β-CDs. At this stage it is useful to consider the fact that during ESI, kinetic trapping of solution phase structures in evaporating droplets and their subsequent transfer to the gas phase is known to occur.[38−40] On the other hand, if the associated barriers on the potential energy surface can be overcome during the electrospray process, then (potentially different) thermodynamically more stable gas-phase structures form. In our case, the barriers for such gas-phase conformational changes associated on the one hand with the hydrogen bond network around a free monomer rim and on the other hand with topology interconversion in oligomers are expected to be widely different. So, a mixture of thermodynamically and kinetically controlled structures might in fact be generated by ESI. Keeping this point in mind, we further considered a HH dimer structure based on the native (open type) structures of β-CD (D2, Figure 3D). This has $^{TM}CCS_{N2}$ of 472 Å^2, which agrees with isomer iii ($^{TIMS}CCS_{N2}$ = 473 Å^2) of $(2{:}1)^{2+}$. We further calculated other possible orientational isomers of $(2{:}1)^{2+}$ by considering different relative orientation between the two β-CDs (open-type). These geometries included HT dimer (D3, $^{TM}CCS_{N2}$ = 473 Å^2, Figure S15A), TT dimer (D4, $^{TM}CCS_{N2}$ = 482 Å^2, Figure S15B), bent geometry with partial inclusion (D5, $^{TM}CCS_{N2}$ = 481 Å^2, Figure S15C), slightly staggered HH (D6, $^{TM}CCS_{N2}$ = 480 Å^2, Figure S15D), more staggered HT (D7, $^{TM}CCS_{N2}$ = 515 Å^2, Figure S15E), perpendicular (D8, $^{TM}CCS_{N2}$ = 509 Å^2, Figure S15F), and a side-by-side (D9, $^{TM}CCS_{N2}$ = 569 Å^2, Figure S15G) orientation between two β-CDs. Although D3−D6 also show $^{TM}CCS_{N2}$ close to that of D2, their possible assignment as isomer iii is less likely as the intermolecular HB interactions are maximized for a HH geometry of the dimer. The other structures D7−D9 showed much larger CCS and hence could be ruled out. Also, dimer formation is driven by the strength of intermolecular interactions. In the case of a free monomer, closing of the primary face stabilizes the structure in the gas-phase by maximizing the intramolecular HBs. However, such a closed monomer is unlikely to contribute to the formation of other orientational topologies such as HT or TT in which the primary rim (T) constitutes the interacting face in the dimer. Thus, we suggest that the most abundant isomer iii of $(2{:}1)^{2+}$ corresponds to a HH dimer (D2) involving condensed-phase like structures of β-CDs. Given its higher relative energy at the PM7 level of 3.16 eV vs D1 (Table S4), we tentatively conclude that D2 is kinetically trapped in the gas-phase (and that the overall topology forms before or in the early stages of the ESI process). Note that a very similar structure has also been observed as a dominant form in crystal structures of β-CD dimers with Cu(II) ions.[12] Also, in the molecular dynamics simulations of gas-phase neutral β-CD dimers by Bonnet et al., retention of the condensed phase-like structures of β-CDs was observed.[14] The smallest isomer i of $(2{:}1)^{2+}$ probably corresponds to a compact closed-type structure of the HH dimer (D1, Figure 3C) which is thermodynamically preferred in the gas-phase. Isomer ii is likely an intermediate state in between these two topologies. Due to the specific patterns of extensive HB interactions present in these systems, the isomers are separated by high barriers which are not overcome under the experimental conditions, and hence both kinetically trapped and thermodynamically controlled forms are observed.

In the case of $(2{:}2)^{2+}$, TIMS MS showed two dominant isomers ($^{TIMS}CCS_{N2}$ = 478 and 482 Å^2). The possible model structures of $(2{:}2)^{2+}$ can be directly compared to calculated structures of $(2{:}1)^{2+}$ for estimating the overall topology as addition of a Cu is not expected to significantly affect the CCS. As a HH dimer shows maximum intermolecular HB interactions, one of the observed isomers of $(2{:}2)^{2+}$ must correspond to a HH dimer like D2 (Figure 3D). The other is likely a different orientational topology in a HT/TT or a slightly staggered HH form. This suggests that in the case of $(2{:}2)^{2+}$, only kinetically trapped structures are observed. Here, an additional Cu ion further strengthens the intermolecular interactions and imparts more structural rigidity to the $(2{:}2)^{2+}$ system compared to that of $(2{:}1)^{2+}$, which probably increases the height of the barriers and prevents structural interconversion into their thermodynamically more stable compact forms in the gas phase. This was further supported by the detection of a slightly populated compact form of $(2{:}2)^{2+}$ at $^{TIMS}CCS_{N2}$ = 449 Å^2 under activated source conditions (Figure S6). The relative population of this compact form of $(2{:}2)^{2+}$ at $^{TIMS}CCS_{N2}$ = 449 Å^2 was raised further (Figure 4) by increasing the effective heating of the ions inside the TIMS tunnel by increasing the voltage (Δ6) between the accumulation and analysis zone of the TIMS setup.[41,42] This compact form of $(2{:}2)^{2+}$ is similar to isomer i of $(2{:}1)^{2+}$ ($^{TIMS}CCS_{N2}$ = 447 Å^2), which further supports our assignment for $(2{:}1)^{2+}$ based on CCS as described earlier. In the case of the other oligomers, increasing the Δ6 voltage did not show a significant effect on the relative population of the isomers

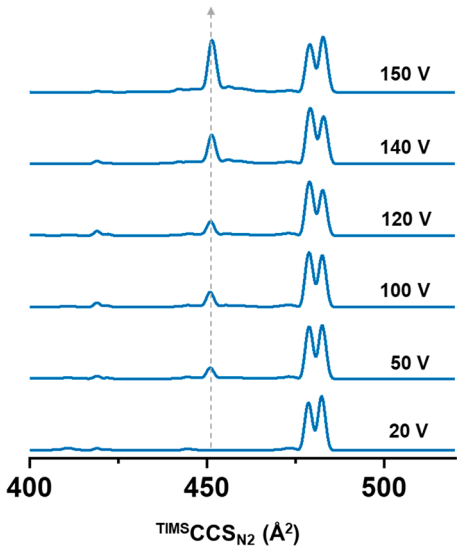

Figure 4. TIMS mobilograms of β-CD $(2:2)^{2+}$ at varying Δ6 voltages. Note the enhancement of the most compact form by collisional heating.

(Figure S16), indicating that the barriers required for structural interconversion are different for the different oligomers.

Isomers of Cu^{2+}-Linked β-CD Trimers. For $(3:1)^{2+}$, one dominant isomer was observed in TIMS MS (584 Å^2). In the solid state, a close-packed "bucket-wheel" shaped trimeric assembly of β-CDs with M^{4+} centers (where M = Mn, Ge, Sn and Pb) was reported by Benner et al.[43] A similar structure of $(3:1)^{2+}$ (T1, Figure 5A) showed $^{TM}CCS_{N2}$ of 582 Å^2, which

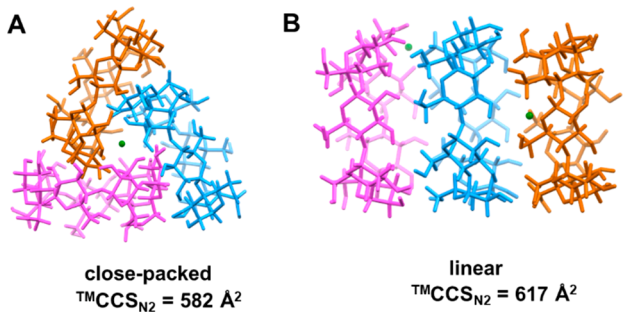

Figure 5. Calculated structures of trimers of β-CD (A) $(3:1)^{2+}$ with compact geometry (T1) and (B) $(3:2)^{3+}$ with a linear channel type geometry, connected in a HT and HT fashion (T′3). Color codes: CD rings are colored in blue/orange/purple for clarity of presentation; green, Cu.

agreed with the experiment ($^{TIMS}CCS_{N2}$ = 584 Å^2). We also calculated additional structures for $(3:1)^{2+}$, in particular structures where the three β-CDs were arranged in a linear (T2, $^{TM}CCS_{N2}$ = 601 Å^2 Figure S17A, Table S5) and side-by-side (T3, $^{TM}CCS_{N2}$ = 736 Å^2, Figure S17B, Table S5) fashion, which were larger compared to the experimental CCS and hence can be ruled out.

A larger number of isomers were observed for $(3:2)^{3+}$ in TIMS MS (Figure 2D). We modeled a similar "bucket-wheel" like structure for $(3:2)^{3+}$ (T′1, Figure S18A, Table S6) which showed $^{TM}CCS_{N2}$ = 604 Å^2, which is close to isomer ii of $(3:2)^{3+}$ ($^{TIMS}CCS_{N2}$ = 592 Å^2, Figure 2D). Isomer i ($^{TIMS}CCS_{N2}$ = 585 Å^2) of $(3:2)^{3+}$ is slightly lower in CCS compared to isomer ii ($^{TIMS}CCS_{N2}$ = 592 Å^2). This indicates that the two isomers i and ii of $(3:2)^{3+}$ likely result from slight changes in the packing of the CDs in the "bucket wheel" like topology. Further, we computed two linear channel-type structures for $(3:2)^{2+}$ where the successive β-CDs were oriented in a T-H...H-T...H-T (T′2,$^{TIMS}CCS_{N2}$ = 613 Å^2 Figure S18B, Table S6) and T-H...T-H...T-H (T′3,$^{TIMS}CCS_{N2}$ = 617 Å^2, Figure 5B, Table S6) fashion. The CCSs of the linear structure T′3 agree with isomer iii ($^{TIMS}CCS_{N2}$ = 623 Å^2) of $(3:2)^{3+}$. Linear channel-type β-CD trimers have also been found to crystallize in the presence of guest molecules.[44] Thus, TIMS MS reveals that $(3:2)^{3+}$ exists as a mixture of linear and close-packed "bucket wheel"-like topologies in gas-phase. Therefore, as already inferred for dimers above, gas-phase trimers can also manifest kinetically trapped structures similar to those in condensed phase.

Isomers of Cu^{2+}-Linked β-CD Tetramers and Pentamers. Due to the larger size, it was computationally more challenging to search for isomeric structures of tetramers and pentamers. So instead, we computed the extreme cases of linear channel type structures for these oligomers and compared their $^{TM}CCS_{N2}$ with experiment to obtain a rough idea of the topologies. For tetramer $(4:2)^{3+}$, a linear channel-type structure (Figure S19A) showed $^{TM}CCS_{N2}$ of 745 Å^2. This was higher than the range of the experimental CCSs of the observed isomers (682−720 Å^2) of $(4:2)^{3+}$. In particular, the major isomers i and ii (682, 688 Å^2) of $(4:2)^{3+}$ were much lower in CCS compared to the calculated linear structure, indicating that Cu-linked β-CD tetramers are mainly present as closely packed assemblies in the gas phase. Similarly, the $^{TM}CCS_{N2}$ of a linear pentamer, $(5:2)^{4+}$ (Figure S19B), was 908 Å^2 which was also much higher than the experimental CCS (838 Å^2 for the largest isomer in TIMS MS). Thus, our study indicates that isolated, Cu^{2+}-linked oligomers with $n > 3$ exist in close-packed topologies.

Cu^{2+}-Linked CD Oligomers: β versus α and γ. Similar but not identical patterns of oligomerization were observed in ESI MS for α-CDs (Figure S20, Table S7) and γ-CDs (Figure S21, Table S8) too. TIMS mobilograms of monomers $(1:0)^{1+}$ and dimers $(2:1)^{2+}$ of α and γ CD, respectively, are presented in Figure 6.

The α-CD monomer $(1:0)^{1+}$ showed a single isomer (Figure 6A), whereas the γ-CD monomer showed two dominant isomers (Figure 6B), which probably reflects the larger flexibility of the γ-CD ring. In both cases, the dimers $(2:1)^{2+}$ showed multiple isomers (Figure 6C,D). Again, the higher flexibility of the γ-CD ring reflects in a larger number of isomers as observed in Figure 6D. The higher oligomers of α- and γ-CD also showed multiple isomers in analogy to the situation for β-CD (Figures S22 and S23 and Tables S7 and S8). However, there was a significant variation in their number and relative intensities depending on the nature of the CDs ($\alpha/\beta/\gamma$), which will be investigated in greater detail in future work.

Growth Pattern of CD Oligomers. To discern growth trends in the early stages of assembly, it is informative to observe measured CCS distributions with oligomer size.[18,20,45] Since the isolated oligomers exist in multiple charge states and exhibit a wide distribution in $^{TIMS}CCS_{N2}$, we correlate the weighted average of the CCS distribution (Ω_{avg}) with the oligomer size (n). Here,

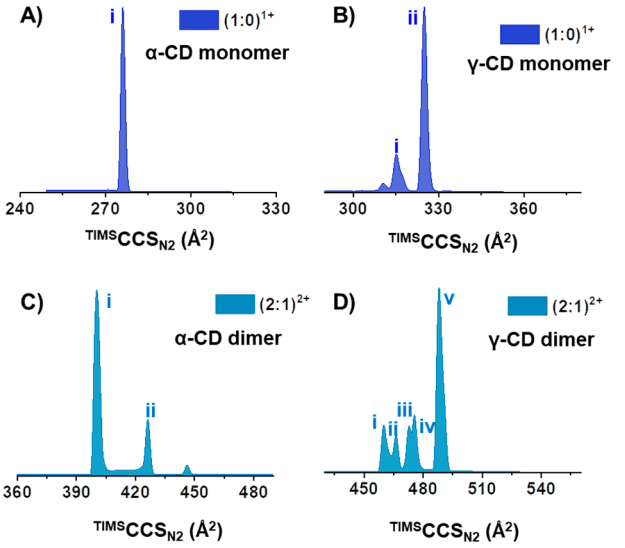

Figure 6. TIMS mobilograms of (A) $(1:0)^{1+}$ α-CD monomer, (B) $(1:0)^{1+}$ γ-CD monomer, (C) $(2:1)^{2+}$ α-CD dimer, and (D) $(2:1)^{2+}$ γ-CD dimer. Oligomers are denoted as $(n{:}m)^{z+}$ where n and m are the number of (correspondingly deprotonated) α/γ-CD and Cu^{2+}, and z is the overall charge state of the species, respectively.

$$\Omega_{avg} = \left(\sum_{i=1}^{n'} I_i \times \Omega_i\right) \Big/ \left(\sum_{i=1}^{n'} I_i\right)$$

where I_i and Ω_i are the relative intensity and CCS of the ith isomer, respectively, and n' is the total number of isomers of all $(n{:}m)^{z+}$ species for a specific size n. Following Haler et al.,[46] we fit Ω_{avg} with a function of the form $\Omega_{avg} = A \times n^p$, where the parameter "$p$" contains the information on the shape of the molecule, and A is a constant (Figure 7). For a perfectly

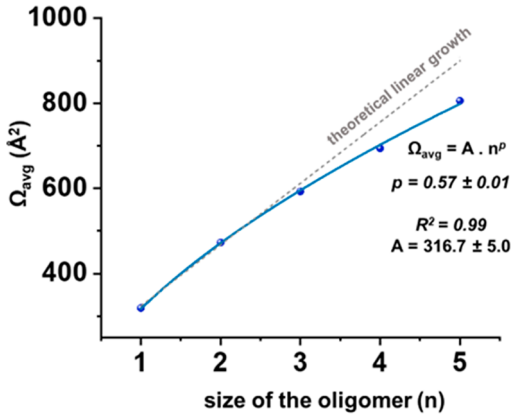

Figure 7. CCS growth curve of β-CD oligomers showing variation of the weighted average of $^{TIMS}CCS_{N2}$ (Å^2) of the isomers as a function of oligomer size, fitted with a power law. A theoretical linear growth trend is indicated for comparison.

spherical geometry p would be 2/3.[18,46] For Cu-linked β-CD assemblies, we find p = 0.57, i.e., a negative deviation from the ideal spherical/isotropic case. This indicates increasingly closely packed assembly with increasing oligomer size[47] possibly arising from partial inclusion between CD rings. Figure 7 compares this behavior to the theoretical CCS growth curve for linear assemblies (predicted using $^{TM}CCS_{N2}$ values of calculated linear structures; see Figure S24 for more details), clearly showing sublinear scaling of the experiment. Fitting the CCS values of α-CD oligomers with the same function leads to p = 0.58 (Figure S25A), similar to the case of β-CD. By contrast for γ-CD (Figure S25B), Ω_{avg} increased almost linearly with increasing n, highlighting the role of the cavity size in controlling the overall growth pattern.

CONCLUSIONS

In summary, we studied Cu^{2+} mediated self-assembly of CDs (α, β, and γ) using ESI MS and high resolution TIMS MS to explore the conformational and topological isomers of the resulting isolated monomers and oligomers. For the Cu-interlinked oligomers, multiple isomers were observed which resulted from topologically distinct patterns of packing of individual CD units, corresponding to both kinetically trapped and thermodynamically controlled structures. For the case of β-CD, we also carried out computational studies to compare $^{TM}CCS_{N2}$ of model oligomeric structures with experimental $^{TIMS}CCS_{N2}$ values and thus assign the corresponding isomer topologies. We further analyzed the overall growth pattern of the Cu-interlinked β-CD oligomers and found that channel type linear structures were not preferred for $n > 3$. Instead, close-packed, partially included forms were predominantly observed for the larger oligomers. Our studies demonstrated how TIMS MS can be used as an effective analytical tool to identify and estimate isomer populations in the complex dynamic system of Cu^{2+}-linked CD oligomers. These studies can also extend to other oligomeric systems of CDs induced by other metal ions or guest molecules. Correspondingly, we hope that our experimental results will stimulate more comprehensive dynamical simulations of this system at higher levels of theory than accessible to us.

The observation of multiple kinetically trapped topologies of isolated CD oligomers in addition to the thermodynamically most stable forms is of potential relevance to the freeze-drying or spray-drying processes used to make amorphous vs crystalline CD powders for industrial applications.[48] A major application of CDs is to trap organic guests for use in various fields like drug delivery, food industry, or cosmetic industry.[49] The efficiency of such trapping processes can be tuned by varying the amorphous to crystalline composition ratio of the CD powders used.[48,50] In future work it will also be of interest to generate novel CD-based materials by soft-landing topology-selected CD oligomers of a given size on surfaces[51] to study isomer-selective applications.

AUTHOR INFORMATION

Corresponding Authors

Papri Chakraborty − *Institute of Nanotechnology, Karlsruhe Institute of Technology, 76344 Eggenstein-Leopoldshafen, Germany; Institute of Physical Chemistry, Karlsruhe Institute of Technology, 76131 Karlsruhe, Germany;* orcid.org/

0000-0002-1353-7734; Email: pc.paprichakraborty@gmail.com

Manfred M. Kappes − *Institute of Nanotechnology, Karlsruhe Institute of Technology, 76344 Eggenstein-Leopoldshafen, Germany; Institute of Physical Chemistry, Karlsruhe Institute of Technology, 76131 Karlsruhe, Germany;* orcid.org/0000-0002-1199-1730; Email: manfred.kappes@kit.edu

Authors

Marco Neumaier − *Institute of Nanotechnology, Karlsruhe Institute of Technology, 76344 Eggenstein-Leopoldshafen, Germany;* orcid.org/0000-0002-3810-3377

Patrick Weis − *Institute of Physical Chemistry, Karlsruhe Institute of Technology, 76131 Karlsruhe, Germany;* orcid.org/0000-0001-7006-6759

Author Contributions

P.C. and M.M. K. conceived the project. P.C. carried out all the experiments and analysis. M.N. carried out the computations. All the authors contributed to the interpretation of the data and wrote the manuscript. The project was supervised by M.M.K.

Notes

The authors declare no competing financial interest.

ACKNOWLEDGMENTS

P.C. thanks Alexander von Humboldt Stiftung/Foundation for her postdoctoral research fellowship. M.M.K. thanks Karlsruhe Institute of Technology (KIT) for funding of the Bruker TIMS TOF instrument used in this project.

REFERENCES

(1) Crini, G. Review: A History of Cyclodextrins. *Chem. Rev.* **2014**, *114*, 10940−10975.

(2) Wankar, J.; Kotla, N. G.; Gera, S.; Rasala, S.; Pandit, A.; Rochev, Y. A. Recent Advances in Host−Guest Self-Assembled Cyclodextrin Carriers: Implications for Responsive Drug Delivery and Biomedical Engineering. *Adv. Funct. Mater.* **2020**, *30*, 1909049.

(3) Szejtli, J. Introduction and General Overview of Cyclodextrin Chemistry. *Chem. Rev.* **1998**, *98*, 1743−1754.

(4) Wenz, G.; Han, B.-H.; Müller, A. Cyclodextrin Rotaxanes and Polyrotaxanes. *Chem. Rev.* **2006**, *106*, 782−817.

(5) Roy, I.; Stoddart, J. F. Cyclodextrin Metal−Organic Frameworks and Their Applications. *Acc. Chem. Res.* **2021**, *54*, 1440−1453.

(6) Harada, A.; Takashima, Y.; Yamaguchi, H. Cyclodextrin-Based Supramolecular Polymers. *Chem. Soc. Rev.* **2009**, *38*, 875−882.

(7) Norkus, E. Metal Ion Complexes with Native Cyclodextrins. An Overview. *J. Incl. Phenom. Macrocycl. Chem.* **2009**, *65*, 237.

(8) Mochida, K.; Matsui, Y. Kinetic Study on the Formation of a Binuclear Complex between Copper(II) and Cyclodextrin. *Chem. Lett.* **1976**, *5*, 963−966.

(9) Kurokawa, G.; Sekii, M.; Ishida, T.; Nogami, T. Short Communication: Crystal Structure of a Molecular Complex from Native β-Cyclodextrin and Copper(II) Chloride. *Supramol. Chem.* **2004**, *16*, 381−384.

(10) Matsui, Y.; Kurita, T.; Date, Y. Complexes of Copper(II) with Cyclodextrins. *Bull. Chem. Soc. Jpn.* **1972**, *45*, 3229−3229.

(11) Bagabas, A. A.; Frasconi, M.; Iehl, J.; Hauser, B.; Farha, O. K.; Hupp, J. T.; Hartlieb, K. J.; Botros, Y. Y.; Stoddart, J. F. γ-Cyclodextrin Cuprate Sandwich-Type Complexes. *Inorg. Chem.* **2013**, *52*, 2854−2861.

(12) Fuchs, R.; Habermann, N.; Klüfers, P. Multinuclear Sandwich-Type Complexes of Deprotonated β-Cyclodextrin. *Angew. Chem., Int. Ed. Engl.* **1993**, *32*, 852−854.

(13) Zhang, H.; Tan, T.; Feng, W.; van der Spoel, D. Molecular Recognition in Different Environments: β-Cyclodextrin Dimer Formation in Organic Solvents. *J. Phys. Chem. B* **2012**, *116*, 12684−12693.

(14) Bonnet, P.; Jaime, C.; Morin-Allory, L. α-, β-, and γ-Cyclodextrin Dimers. Molecular Modeling Studies by Molecular Mechanics and Molecular Dynamics Simulations. *J. Org. Chem.* **2001**, *66*, 689−692.

(15) Lanucara, F.; Holman, S. W.; Gray, C. J.; Eyers, C. E. The Power of Ion Mobility-Mass Spectrometry for Structural Characterization and the Study of Conformational Dynamics. *Nat. Chem.* **2014**, *6*, 281−294.

(16) Jurneczko, E.; Barran, P. E. How Useful Is Ion Mobility Mass Spectrometry for Structural Biology? The Relationship between Protein Crystal Structures and Their Collision Cross Sections in the Gas Phase. *Analyst* **2011**, *136*, 20−28.

(17) Bohrer, B. C.; Merenbloom, S. I.; Koeniger, S. L.; Hilderbrand, A. E.; Clemmer, D. E. Biomolecule Analysis by Ion Mobility Spectrometry. *Annu. Rev. Anal. Chem. (Palo Alto, Calif.)* **2008**, *1*, 293−327.

(18) Bleiholder, C.; Dupuis, N. F.; Wyttenbach, T.; Bowers, M. T. Ion Mobility−Mass Spectrometry Reveals a Conformational Conversion from Random Assembly to β-Sheet in Amyloid Fibril Formation. *Nat. Chem.* **2011**, *3*, 172−177.

(19) Le Fèvre, A.; Dugourd, P.; Chirot, F. Exploring Conformational Landscapes Using Trap and Release Tandem Ion Mobility Spectrometry. *Anal. Chem.* **2021**, *93*, 4183−4190.

(20) Do, T. D.; Kincannon, W. M.; Bowers, M. T. Phenylalanine Oligomers and Fibrils: The Mechanism of Assembly and the Importance of Tetramers and Counterions. *J. Am. Chem. Soc.* **2015**, *137*, 10080−10083.

(21) Kalenius, E.; Groessl, M.; Rissanen, K. Ion Mobility−Mass Spectrometry of Supramolecular Complexes and Assemblies. *Nat. Rev. Chem.* **2019**, *3*, 4−14.

(22) Polewski, L.; Springer, A.; Pagel, K.; Schalley, C. A. Gas-Phase Structural Analysis of Supramolecular Assemblies. *Acc. Chem. Res.* **2021**, *54*, 2445−2456.

(23) Przybylski, C.; Bonnet, V. Probing Topology of Supramolecular Complexes between Cyclodextrins and Alkali Metals by Ion Mobility-Mass Spectrometry. *Carbohydr. Polym.* **2022**, *297*, 120019.

(24) Rabus, J. M.; Pellegrinelli, R. P.; Khodr, A. H. A.; Bythell, B. J.; Rizzo, T. R.; Carrascosa, E. Unravelling the Structures of Sodiated β-Cyclodextrin and Its Fragments. *Phys. Chem. Chem. Phys.* **2021**, *23*, 13714−13723.

(25) Zimnicka, M.; Troć, A.; Ceborska, M.; Jakubczak, M.; Koliński, M.; Danikiewicz, W. Structural Elucidation of Specific Noncovalent Association of Folic Acid with Native Cyclodextrins Using an Ion Mobility Mass Spectrometry and Theoretical Approach. *Anal. Chem.* **2014**, *86*, 4249−4255.

(26) Chouinard, C. D.; Nagy, G.; Webb, I. K.; Garimella, S. V. B.; Baker, E. S.; Ibrahim, Y. M.; Smith, R. D. Rapid Ion Mobility Separations of Bile Acid Isomers Using Cyclodextrin Adducts and Structures for Lossless Ion Manipulations. *Anal. Chem.* **2018**, *90*, 11086−11091.

(27) Ridgeway, M. E.; Lubeck, M.; Jordens, J.; Mann, M.; Park, M. A. Trapped Ion Mobility Spectrometry: A Short Review. *Int. J. Mass Spectrom.* **2018**, *425*, 22−35.

(28) Michelmann, K.; Silveira, J. A.; Ridgeway, M. E.; Park, M. A. Fundamentals of Trapped Ion Mobility Spectrometry. *J. Am. Soc. Mass Spectrom.* **2015**, *26*, 14−24.

(29) Stow, S. M.; Causon, T. J.; Zheng, X.; Kurulugama, R. T.; Mairinger, T.; May, J. C.; Rennie, E. E.; Baker, E. S.; Smith, R. D.; McLean, J. A.; Hann, S.; Fjeldsted, J. C. An Interlaboratory Evaluation of Drift Tube Ion Mobility−Mass Spectrometry Collision Cross Section Measurements. *Anal. Chem.* **2017**, *89*, 9048−9055.

(30) Stewart, J. J. Optimization of Parameters for Semiempirical Methods VI: More Modifications to the NDDO Approximations and Re-Optimization of Parameters. *J. Mol. Model* **2013**, *19*, 1−32.
(31) Stewart, J. J. Mopac: A Semiempirical Molecular Orbital Program. *J. Comput. Aided Mol. Des.* **1990**, *4*, 1−105.
(32) Larriba, C.; Hogan, C. J. Ion Mobilities in Diatomic Gases: Measurement Versus Prediction with Non-Specular Scattering Models. *J. Phys. Chem. A* **2013**, *117*, 3887−3901.
(33) Kim, H.; Kim, H. I.; Johnson, P. V.; Beegle, L. W.; Beauchamp, J. L.; Goddard, W. A.; Kanik, I. Experimental and Theoretical Investigation into the Correlation between Mass and Ion Mobility for Choline and Other Ammonium Cations in N_2. *Anal. Chem.* **2008**, *80*, 1928−1936.
(34) Klein, C.; Cologna, S. M.; Kurulugama, R. T.; Blank, P. S.; Darland, E.; Mordehai, A.; Backlund, P. S.; Yergey, A. L. Cyclodextrin and Malto-Dextrose Collision Cross Sections Determined in a Drift Tube Ion Mobility Mass Spectrometer Using Nitrogen Bath Gas. *Analyst* **2018**, *143*, 4147−4154.
(35) Naidoo, K. J.; Gamieldien, M. R.; Chen, J. Y.-J.; Widmalm, G.; Maliniak, A. Glucose Orientation and Dynamics in α-, β-, and γ-Cyclodextrins. *J. Phys. Chem. B* **2008**, *112*, 15151−15157.
(36) Stachowicz, A.; Styrcz, A.; Korchowiec, J.; Modaressi, A.; Rogalski, M. DFT Studies of Cation Binding by β-Cyclodextrin. *Theor. Chem. Acc.* **2011**, *130*, 939−953.
(37) Karpfen, A.; Liedl, E.; Snor, W.; Weiss-Greiler, P.; Viernstein, H.; Wolschann, P. Homodromic Hydrogen Bonds in Low-Energy Conformations of Single Molecule Cyclodextrins. *J. Incl. Phenom. Macrocycl. Chem.* **2007**, *57*, 35−38.
(38) Patrick, A. L.; Cismesia, A. P.; Tesler, L. F.; Polfer, N. C. Effects of ESI Conditions on Kinetic Trapping of the Solution-Phase Protonation Isomer of p-Aminobenzoic Acid in the Gas Phase. *Int. J. Mass Spectrom.* **2017**, *418*, 148−155.
(39) Fort, K. L.; Silveira, J. A.; Pierson, N. A.; Servage, K. A.; Clemmer, D. E.; Russell, D. H. From Solution to the Gas Phase: Factors That Influence Kinetic Trapping of Substance P in the Gas Phase. *J. Phys. Chem. B* **2014**, *118*, 14336−14344.
(40) Silveira, J. A.; Fort, K. L.; Kim, D.; Servage, K. A.; Pierson, N. A.; Clemmer, D. E.; Russell, D. H. From Solution to the Gas Phase: Stepwise Dehydration and Kinetic Trapping of Substance P Reveals the Origin of Peptide Conformations. *J. Am. Chem. Soc.* **2013**, *135*, 19147−19153.
(41) Morsa, D.; Hanozin, E.; Eppe, G.; Quinton, L.; Gabelica, V.; Pauw, E. D. Effective Temperature and Structural Rearrangement in Trapped Ion Mobility Spectrometry. *Anal. Chem.* **2020**, *92*, 4573−4582.
(42) Borotto, N. B.; Osho, K. E.; Richards, T. K.; Graham, K. A. Collision-Induced Unfolding of Native-Like Protein Ions within a Trapped Ion Mobility Spectrometry Device. *J. Am. Soc. Mass Spectrom.* **2022**, *33*, 83−89.
(43) Benner, K.; Ihringer, J.; Klüfers, P.; Marinov, D. Cyclodextrin Bucket Wheels: An Oligosaccharide Assembly Accommodates Metal(IV) Centers. *Angew. Chem., Int. Ed.* **2006**, *45*, 5818−5822.
(44) Chatziefthimiou, S. D.; Yannakopoulou, K.; Mavridis, I. M. β-Cyclodextrin Trimers Enclosing an Unusual Organization of Guest: The Inclusion Complex β-Cyclodextrin/4-Pyridinealdazine. *CrystEngComm* **2007**, *9*, 976−979.
(45) Bleiholder, C.; Bowers, M. T. The Solution Assembly of Biological Molecules Using Ion Mobility Methods: From Amino Acids to Amyloid β-Protein. *Annu. Rev. Anal. Chem.* **2017**, *10*, 365−386.
(46) Haler, J. R. N.; Béchet, E.; Kune, C.; Far, J.; De Pauw, E. Geometric Analysis of Shapes in Ion Mobility−Mass Spectrometry. *J. Am. Soc. Mass Spectrom.* **2022**, *33*, 273−283.
(47) Do, T. D.; de Almeida, N. E. C.; LaPointe, N. E.; Chamas, A.; Feinstein, S. C.; Bowers, M. T. Amino Acid Metaclusters: Implications of Growth Trends on Peptide Self-Assembly and Structure. *Anal. Chem.* **2016**, *88*, 868−876.
(48) Ho, T. M.; Howes, T.; Bhandari, B. R. Characterization of Crystalline and Spray-Dried Amorphous α-Cyclodextrin Powders. *Powder Technol.* **2015**, *284*, 585−594.
(49) Sharma, N.; Baldi, A. Exploring Versatile Applications of Cyclodextrins: An Overview. *Drug Delivery* **2016**, *23*, 729−747.
(50) Ho, T. M.; Truong, T.; Bhandari, B. R. Methods to Characterize the Structure of Food powders − a Review. *Biosci. Biotechnol. Biochem.* **2017**, *81*, 651−671.
(51) Mikhailov, V. A.; Mize, T. H.; Benesch, J. L. P.; Robinson, C. V. Mass-Selective Soft-Landing of Protein Assemblies with Controlled Landing Energies. *Anal. Chem.* **2014**, *86*, 8321−8328.